JOURNAL OF GEOPHYSICAL RESEARCH, VOL. 104, NO. E4, PAGES 8957–8974, APRIL 25, 1999

General circulation model simulations of the Mars Pathfinder atmospheric structure investigation/meteorology data

Robert M. Haberle,[1] Manoj M. Joshi,[1] James R. Murphy,[2,3]
Jeffrey R. Barnes,[4] John T. Schofield,[5] Greg Wilson,[6,7]
Miguel Lopez-Valverde,[8] Jeffery L. Hollingsworth,[2]
Alison F. C. Bridger,[9] and James Schaeffer[10,11]

Abstract. The NASA Ames Mars General Circulation Model is used to interpret selected results from the Mars Pathfinder atmospheric structure instrument/meteorology (ASI/MET) experiment. The present version of the model has an improved soil thermal model, a new boundary layer scheme, and a correction for non–local thermodynamic equilibrium effects at solar wavelengths. We find good agreement with the ASI/MET entry data if the dust observed at the Pathfinder site is assumed to be distributed throughout the lowest five to six scale heights. This implies that the dust is globally distributed as well. In the lower atmosphere the inversion between 10 and 16 km in Pathfinder's entry profile is likely due to thermal emission from a water ice cloud in that region. In the upper atmosphere (above 50 km), dynamical processes, tides in particular, appear to have a cooling effect and may play an important role in driving temperatures toward the CO_2 condensation temperature near 80 km. Near-surface air temperatures and wind directions are well simulated by the model by assuming a low surface albedo (0.16) and moderately high soil thermal inertia (336 SI). However, modeled tidal surface pressure amplitudes are about a factor of 2 smaller than observed. This may indicate that the model is not properly simulating interference effects between eastward and westward modes.

1. Introduction

The Mars Pathfinder spacecraft successfully landed on the surface of Mars in the Ares Vallis floodplain (19.17°N, 33.21°W) on July 4, 1997. The landing took place at 0258 true local solar time. The seasonal date was $L_s = 142°$ in mid-northern summer. (L_s is an angular measure of the planet's orbital position; $L_s = 0°$ corresponds to northern spring equinox, 90° to northern summer solstice, 180° to northern fall equinox, and 270° to northern winter solstice.) The spacecraft carried a suite of instruments, including a rover that gathered data to address a variety of science objectives. Science data were returned up through sol 83 ($L_s = 187°$) and totaled over 2 Gbits of new data. (A "sol" is a Martian solar day; 1 sol = 88,775 s). The last communication with Pathfinder occurred on October 7, 1997 ($L_s = 194°$), but there was no telemetry. *Golombek et al.* [this issue] give a detailed overview of the Pathfinder mission.

In this paper, we use the NASA Ames Mars general circulation model (MGCM) to simulate Pathfinder's entry and landed meteorology data. These data were collected by the atmospheric structure investigation/meteorology (ASI/MET) experiment, whose objectives and instrumentation are described by *Seiff et al.* [1997]. The entry data consist of a single temperature profile, which was deduced from three-axis accelerometer measurements. The landed data consists of wind, temperature, and pressure measurements, though at the present time, wind speed data are not available. *Schofield et al.* [1997] discuss the preliminary results of Pathfinder's ASI/MET experiment.

Our goal is to use the MGCM as a tool for interpreting the ASI/MET data. We begin in the next section with a brief description of the data and then assess our earlier MGCM prediction of the meteorological conditions Pathfinder might encounter [*Haberle et al.*, 1997]. Since the prediction paper, we have upgraded the representation of various physical processes in the model, and we describe these in section 4. Section 5 deals with our experimental procedure and adopted model parameters. We then give an overview of the simulated global circulation during the Pathfinder mission in section 6, and then compare the main results of our simulations with Pathfinder data in sections 7 and 8. We follow this with discussion in section 9 and conclusions in section 10.

2. ASI/MET Data Set

The ASI part of Pathfinder's ASI/MET experiment operated during the entry, descent, and landing phase of the mission. It was based on deceleration measurements from a three-axis

[1]Space Science Division, Ames Research Center, Moffett Field, California.
[2]San Jose State University Foundation, San Jose, California.
[3]Now at Department of Astronomy, New Mexico State University, Las Cruces.
[4]College of Oceanic and Atmospheric Sciences, Oregon State University, Corvallis.
[5]Jet Propulsion Laboratory, Pasadena, California.
[6]Geology Department, Arizona State University, Tempe.
[7]Now at Jet Propulsion Laboratory, Pasadena, California.
[8]Instituto de Astrofisica de Andalucia, Granada, Spain.
[9]Department of Meteorology, San Jose State University, San Jose, California.
[10]Sterling Software, Palo Alto, California.
[11]Now at Raytheon, Moffett Field, California.

Paper number 1998JE900040.
0148-0227/99/1998JE900040$09.00

Table 1. Comparison of Predicted and Observed Meteorological Parameters

Parameter	Predicted	Observed
Visible dust optical depth	0.3–0.6 (not based on MGCM)	0.4–0.6
Entry temperature profile	like Viking	below 50 km, like Viking; above 50 km, cooler than Viking
Surface air temperature	185–250 K	200–260 K
Surface pressure	not predicted because of unknown topography	6.76 mbar (daily average)
Surface wind speed	2–10 m/s	not yet reported
Surface wind direction	upslope/downslope rotating clockwise	upslope/downslope rotating clockwise
Basic weather pattern	regular and repetitive	regular and repetitive
Daily pressure variation	strong semidiurnal component	strong semidiurnal component
Daily mean pressure trend	falling	falling
Time of pressure minimum	20 sols after landing	22 sols after landing
Time of transition to winter weather pattern	60 sols after landing	80 sols after landing

accelerometer. Deceleration can be related to atmospheric density, given the spacecraft's aerodynamic characteristics, which were determined prior to launch, and the flight path trajectory, which was reconstructed from observed decelerations and an assumed initial position and velocity. A pressure profile can then be derived from the density profile by integrating the hydrostatic equation, and from this a temperature profile is obtained by applying the equation of state. Details are given by *Magalhaes et al.* [this issue].

The sensitivity of the accelerometers (20 $\mu m/s^2$) and the rapid rate at which they were sampled (32 Hz) allowed reconstruction of the temperature profile from 160 to 9 km with a vertical resolution of 250 m at the beginning of entry to 25 m at the end. Temperatures below 9 km, where the parachute was deployed, have not yet been determined. In the region of interest for our purposes (0–80 km), the reconstructed temperature profile has uncertainties of ±1 K.

The MET part of the ASI/MET experiment began after the spacecraft landed and continued until the end of the mission. The wind and temperature measurements were conducted by sensors mounted on a 1.1 m mast, which was deployed at the end of the southeast lander petal, itself estimated to be about 0.27 m above the "mean" ground level (R. Kirk, personal communication, 1998). Three of the four thermocouples along the mast were designed for surface meteorological studies. These were positioned at 0.25, 0.5, and 1.0 m above the bottom of the mast. Thus they measured temperatures at 0.52, 0.77, and 1.27 m above the ground. The wind sensor, a six-segment heated wire device, was mounted at the top of the mast. The pressure sensors were located inside the lander's thermal enclosure and were exposed to the atmosphere via a 1 m inlet tube.

The nominal sampling strategy for the MET experiment was designed to capture the full diurnal cycle with 51 equally spaced 3 min sessions per sol. Within each of these sessions, the meteorological fields were sampled at 4 s intervals. Interspersed among these were rotating 15 min and 1 hour sessions with 1 s sampling. These sessions were designed to emphasize boundary layer processes. Finally, on five of Pathfinder's 83 sols (sols 25, 32, 38, 55, and 68), meteorological data were acquired continuously at 4 s intervals for the entire sol.

During the primary mission (sols 1–30), spacecraft resets and MET software errors interrupted the regular sessions, so that good diurnal coverage was not possible on 10 of the first 30 sols. During the extended mission (sols 31–83), declining battery capacity often limited operations to daytime hours only, so that for this period, only 4 sols have good diurnal coverage.

After the preliminary results were published [*Schofield et al.*, 1997], the temperature dependence of the pressure sensor offset was reassessed. An improved temperature calibration was derived and applied to the data. Details are given in the appendix. In this paper, we utilize this recalibrated pressure data. As will be discussed, the main impact of the new calibration is to significantly increase the observed diurnal tidal amplitudes.

3. MGCM Prediction Assessment

Just prior to Pathfinder's landing, we published a paper predicting the meteorological conditions the spacecraft would encounter for both the entry and landed phases [*Haberle et al.*, 1997]. Here we assess how well those predictions fared.

Table 1 summarizes the results. As predicted, the optical depth, entry profile, daily pressure variation, and winds were very much like those observed by Viking Lander 1 (VL-1) at the same season [*Smith et al.*, 1997; *Schofield et al.*, 1997]. There were, however, some surprises: the generally cooler (~20 K) atmosphere above 50 km, the presence of an elevated temperature inversion between 9 and 16 km, and the much warmer (10–15 K) near-surface air temperatures. We shall address each of these later.

It is important to point out that our predicted optical depth was not based on MGCM simulations. Instead, it was based on our belief that Pathfinder would encounter conditions very similar to those observed by VL-1 21 years earlier. Indeed, this was the case. We were aware of the Earth-based microwave observations that have been interpreted in terms of a much clearer and colder atmosphere at this season compared to Viking [*Clancy et al.*, 1996], and we carefully considered this possibility. However, in the end we placed highest priority on in situ measurements and opted for a "persistence" forecast. In this sense, we were truly forecasting like weather forecasters do for Earth when confronted with conflicting data and/or model simulations.

While Pathfinder did find warm, dusty, Viking-like conditions, these findings are difficult to reconcile with the Earth-based microwave observations which were taken just before and just after Pathfinder landed (T. Clancy, unpublished data, 1997). Those observations continued to show a non-Viking-like cooler, clearer climate. Could it be that the Pathfinder and Viking landing sites are anomalous? We argue against this in the Discussion (section 9). However, the issue remains unresolved and puzzling, particularly since the microwave observa-

tions taken after the Pathfinder mission ended agree quite well those from the thermal emission spectrometer (TES) instrument aboard the Mars Global Surveyor (MGS) orbiter taken during the following fall/winter season (T. Clancy, personal communication, 1998). We hope to learn more on this issue when TES observes Mars during the northern summer season.

4. Model Upgrades

We have made several improvements to the MGCM since our prediction paper. First, we have included a new boundary layer scheme. This new scheme, adapted from *Haberle et al.* [1993], is based on turbulence closure corresponding to the "level 2" hierarchy of models in the *Mellor and Yamada* [1982] classification. The modifications to the Haberle et al. model were made to simplify the computations and improve its numerical stability; they have very little effect on the predicted fields. Specifically, we changed the way we calculate the surface fluxes and eddy mixing coefficients. The surface fluxes are now calculated from

$$\tau = \rho u_*^2$$

$$H = -\rho c_p u_* \theta_*$$

where u_* and θ_* are defined in terms of the mean wind u and air-to-ground temperature difference $\Delta\Theta$ from the relations

$$u_* = (C_{dm})^{1/2} u$$

$$\theta_* = C_{dh}\Delta\Theta$$

with the drag coefficients being given by

$$C_{dm} = F_m\left(\frac{k}{\ln (z/z_0)}\right)^2$$

$$C_{dh} = (F_h)^{1/2}\frac{k}{\ln (z/z_0)}$$

In these expressions, F_m and F_h are stability functions (the subscripts m and h refer to momentum and heat, respectively), k is the von Karman constant (0.4), z is the height of the lowest model layer (5 m), and z_0 is the roughness length, which we take to be 1 cm everywhere. The stability functions F_h and F_m are taken from *Savijarvi* [1995] when the Richardson number Ri is less than zero,

$$F_m = (1 - 64Ri)^{1/2}$$

$$F_h = (1 - 16Ri)^{1/2}$$

and from *Hourdin et al.* [1995] when $Ri > 0$,

$$F_m = \{1 + [10Ri/(1 + 5Ri)^{1/2}]\}^{-1}$$

$$F_h = \{1 + [15Ri/(1 + 5Ri)^{1/2}]\}^{-1}$$

The calculation of the eddy mixing coefficients is now based on functions derived by *Arya* [1988]. When $Ri < 0$,

$$K_m = K_{m0}(1 - 15Ri)^{1/4}$$

$$K_h = K_{h0}(1 - 15Ri)^{1/2}$$

while for $Ri > 0$,

$$K_m = K_{m0}\left(1 - \frac{Ri}{Ri_c}\right)$$

$$K_h = K_{h0}\left(1 - \frac{Ri}{Ri_c}\right)$$

where the neutral eddy coefficients are given in terms of the wind shear $\partial u/\partial z$ and the mixing length l by

$$K_{m0} = S_m l^2 \left(\frac{\partial u}{\partial z} G_m^{-1}\right)^{1/2}$$

$$K_{h0} = S_h l^2 \left(\frac{\partial u}{\partial z} G_m^{-1}\right)^{1/2}$$

For neutral conditions the level 2 theory gives $S_m = 0.393$, $S_h = 0.493$, and $G_m = 0.153$. The mixing length is calculated as before and asymptotes to $l_0 = 150$ m.

In the level 2 hierarchy of models the eddy coefficients vanish when $Ri > Ri_c$, a critical Richardson number we take to be 0.20. In the present version, we do not allow the eddy coefficients to fall below 0.1 m^2/s. This gives smoother nighttime solutions and is more consistent with the fact that turbulence is not instantaneously extinguished.

We found when the original version of the new scheme was incorporated into the MGCM, nighttime 2 Δt oscillations developed in the mixing coefficients near the top of the boundary layer when it collapsed in the late afternoon. These oscillations were traced to the larger time step used by the MGCM compared to the original boundary layer model, and the basic assumption in level 2 schemes that the production and dissipation of turbulent kinetic energy are always balanced. We were able to eliminate this numerical oscillation by smoothing the wind shear used to calculate the bulk Richardson number (and hence the mixing coefficients) over a timescale of 3–6 hours. This modification was found to have a minimal effect on the evolution of the wind and temperature fields.

In addition to incorporating this modified version of the *Haberle et al.* [1993] boundary layer scheme into the MGCM, we have also included a 12-layer soil model based on the work of *Haberle and Jakosky* [1991]. The model uses standard numerical techniques to solve the thermal diffusion equation. The layers increase in thickness with depth, with the first layer being 0.75 cm thick, while the last layer is 5 cm thick. The total depth is 26 cm. This is deep enough to capture the diurnal wave but not the annual wave.

In the present version of the model, we run with 30 vertical atmospheric layers and a model top ("tropopause") at the 20 nbar level (~95 km). We wish to run with the model top as high as possible to facilitate comparison with the Pathfinder entry data. Furthermore, *Wilson* [1997] has suggested that a deep domain is required to reasonably simulate wintertime polar warming phenomena, and experiments with our model have verified this assertion.

However, non-local thermodynamic equilibrium (LTE) effects begin to become important at altitudes above 80 km [*Lopez-Valverde et al.*, 1998]. Therefore, we have included the correction function to LTE solar heating rates recommended by *Lopez-Valverde et al.* [1998]. In effect, our LTE solar heating rates are multiplied by a factor

$$f = \frac{2.2 \times 10^4 p}{(1 + 2.2 \times 10^4 p)}$$

where p is in millibars. This function is a fit to the tabular data provided by Lopez-Valverde et al. At 100 nbar the multiplying

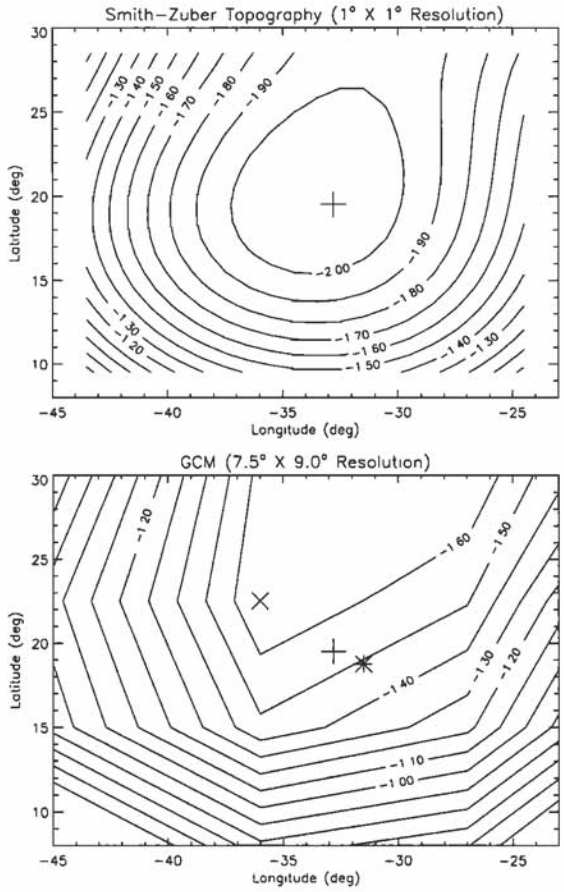

Figure 1. Smith-Zuber topography (kilometers) centered around the Pathfinder landing site. (top) Original 1° × 1° data set. (bottom) Same as top but plotted at MGCM resolution (7.5° × 9°). Contour interval is 0.1 km. Plus symbol signifies the actual Pathfinder landing site. The cross and asterisk signify GCM grid points; temperature and pressure are predicted at the cross, while the horizonal wind components (u, v) are predicted at the asterisk.

factor is ~0.7; at 20 nbar the factor is ~0.3. At the present time, there is no correction for non-LTE effects in the infrared. While errors associated with not having a correction in the infrared are anticipated to be less than those without one at solar wavelengths, it is still a matter of concern.

5. Model Parameters and Experiment Procedure

For this paper the model is configured to run with 25 latitude points, 40 longitude points, and 30 vertical layers from the surface to 20 nbar. The horizontal resolution is 7.5° latitude, 9° longitude. Vertically, the resolution varies, and layer thicknesses increase with height. Our lowest model layer is ~10 m thick, so that wind and temperature are predicted at about the 5 m level.

We use the topographic data set derived by *Smith and Zuber* [1996]. This data set incorporates Viking occultation data and represents the best available fit to the long wavelength figure of the planet, though there is still some concern about the polar regions [*Forget and Pollack*, 1996]. A section of that data set centered around the Pathfinder landing site, along with the corresponding field at the MGCM's resolution, is shown in Figure 1. Note in this figure that the MGCM grid points carrying wind are staggered from those carrying temperature/pressure and that neither coincides with the Pathfinder landing site. When comparing the MGCM results to Pathfinder, we simply use the grid point closest to the landing site. No interpolation is performed.

The albedo and thermal inertia we use are based on the Consortium data set but modified as follows. First, we account for the effect of dust on derived thermal inertias as described by *Hayashi et al.* [1995]. For a dust visible optical depth of 0.5, the actual surface thermal inertia is about 20% less than those in the Consortium data. We adopt this reduction uniformly over the planet. For the albedo, however, *Hayashi et al.* [1995] find that at this opacity it should be increased slightly (~0.03) in order to reproduce Viking infrared thermal mapper (IRTM) 20 μm temperatures (taken to be surface temperature). We have found that raising the Consortium albedos gives temperatures at the Pathfinder site that are much cooler than observed. Better agreement is obtained by actually reducing the Consortium albedos. Therefore we applied an ad hoc uniform reduction in the Consortium albedos of 0.05. For the Pathfinder landing site the modified albedo and thermal inertia are 0.16 and 336 SI units, respectively.

The need to decrease the albedo may be due to the fact that there are large variations in the local albedo within the Ares Vallis region and that the spacecraft happened to land in a relatively dark region. *Edgett and Christensen* [1997] report albedos as low as 0.19 within the landing ellipse. This is at least consistent with the lower ad hoc value we require.

In our prediction paper, we chose surface properties that gave the best fit to the VL-1 nighttime air temperatures and the 20 μm IRTM daytime temperatures. The latter were similar for the Pathfinder and VL-1 sites, though the coverage was limited. Consequently, our predicted daily temperature variation of 185–250 K was similar to that at VL-1. However, the observed temperatures were much warmer and varied from 200 to 260 K. Thus the surface properties at the Pathfinder site may not be representative of those producing the measured 20 μm brightness temperatures.

Our polar cap properties are taken from *Hourdin et al.* [1995], who carried out a comprehensive study of the present seasonal CO_2 cycle and its dependence on a wide variety of atmospheric and surface properties. We chose these values, since they give the least rms error when compared to the Viking Lander 1 pressure data. Accordingly, the cap albedos are 0.64 for the north cap and 0.40 for the south cap, while the cap emissivities are 0.47 for the north cap and 0.70 for the south cap [see *Hourdin et al.*, 1995, Table 4]. With these values, we obtain a good fit to the VL-1 pressure measurements if we assume that the total amount of CO_2 in the system is 7.72 mbar. This is different from the 6.58 mbar quoted by Hourdin et al. because they conducted their simulations using digital terrain mapping (DTM) topography, whereas we are using the Smith/Zuber data set.

In the simulations reported here, we prescribe the atmospheric dust loading. Spatially, we assume the dust is uniformly mixed in the horizontal but falls off exponentially with height according to the prescription given by *Conrath* [1975]:

$$q = q_0 \exp\left[\nu\left(1 - \frac{\bar{P}}{P}\right)\right] \qquad P \le \bar{P}$$

$$q = q_0 \qquad P > \bar{P}$$

where q is the dust mixing ratio, q_0 is a constant determined by the dust optical depth at the pressure level corresponding to the globally averaged surface pressure $\bar{P}$, and ν is a free parameter that determines the effective depth of the dust. Some examples of the profiles we use are shown in Figure 2. Our standard run employs $\nu = 0.003$, which was tuned to give a good match to the entry data. From Figure 2, this indicates that the dust mixing ratio declines to 50% of its surface value at five to six scale heights and is virtually zero by seven to eight scale heights.

The optical properties used to compute dust infrared emissivities were taken from *Toon et al.* [1977] and are known to yield a visible-to-infrared optical depth ratio of ~1. This value is about a factor of 2 smaller than the observed value [*Martin*, 1986]. We account for this discrepancy by reducing the optical depth by a factor of 2 when computing the dust infrared emissivity. This approach was found to give a better representation of the dust "greenhouse" effect [*Haberle and Jakosky*, 1991], but it is crude. However, several simulations with the MGCM (not shown) indicate that as long as the dust is optically thin in the visible (opacities <1), the visible-to-infrared extinction efficiency does not have a major effect on atmospheric temperatures.

Our assumed temporal variation of dust opacity is based on a linear fit to the midday Pathfinder 0.67 μm opacities as shown in Figure 3. This wavelength is the same as the Viking Sun diode observations. We limit the data to midday to get a better representation of the dust opacity, since morning water ice clouds were occasionally observed [*Smith et al.*, 1997]. The fitted values shown in Figure 3 (solid line) correspond to the actual values at the MGCM temperature/pressure grid point closest to the Pathfinder landing site. In the Smith/Zuber data set the Pathfinder site is about 1.7 km below the globally averaged elevation (at MGCM resolution). Thus, assuming the dust is uniformly distributed horizontally, the global optical depth would be about 25% lower than that shown in Figure 3. At the end of the Pathfinder mission the measured visible opacities were ~0.60, which would therefore correspond to a global opacity of ~0.45. When scaled to 9 μm, this value is consistent with those inferred from TES aboard MGS, which arrived at Mars in mid-September of 1997, about 2 weeks before the end of the Pathfinder mission [*Christensen et al.*, 1998].

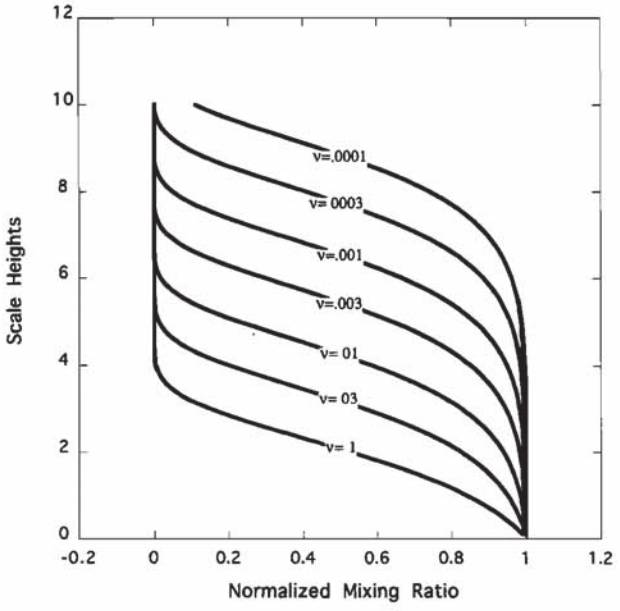

Figure 2. Sample dust profiles used in the MGCM. The mixing ratio is normalized by its surface value q_0. The ν parameter determines the depth of dust. For our nominal run, $\nu = 0.003$. See text for details.

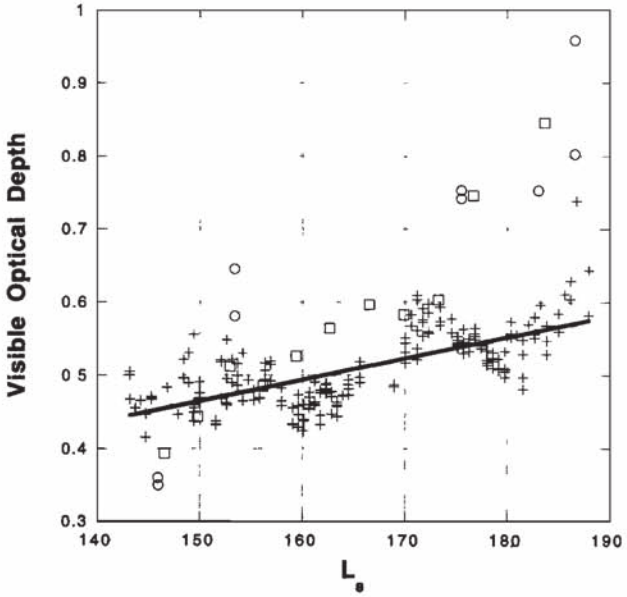

Figure 3. Viking and Pathfinder opacities. The Pathfinder data (crosses) represent the 0.67 μm filter camera measurements [see *Smith et al.*, 1997] and were restricted to measurements taken between 1000 and 1400 local time. The Viking data represent the Sun diode measurements [see *Colburn et al.*, 1989], which also correspond to a wavelength of 0.67 μm. These data were taken in the afternoon (generally between 1500 and 1600 hours). The first-year data are the open circles; the second-year data are the open squares.

Since Pathfinder appears to be at nearly the same elevation as VL-1 (Pathfinder is ~60 m higher than VL-1 based on ranging data) and since it is only about 800 km from the VL-1 site, it is worth comparing its opacities with those observed by VL-1 at the same season. This comparison is also given in Figure 3 (note that Viking data are also afternoon data). For the period $L_s = 142°$–$175°$, Pathfinder opacities are not significantly different from those measured by VL-1. However, after $L_s = 175°$, they are significantly different, in spite of the poor temporal coverage in the Viking data. In particular, Pathfinder opacities do not rise as quickly with the approach of fall as do those observed by VL-1. For the period $L_s = 175°$–$187°$, VL-1 opacities were between 0.75 and 0.95 for the first and second year, while at the Pathfinder site they were between 0.50 and 0.65. Interpreting these differences in terms of regional versus global variability is not possible without additional observations, but it does further emphasize the dynamic nature of the Martian atmosphere during the northern fall/winter season.

With the upgrades and parameters described above, we run our standard model from a cold start (isothermal atmosphere, no CO_2 ice on the ground) at $L_s = 0°$ to $L_s = 187°$. The opacity history prior to $L_s = 142°$ is taken from VL-1. By starting at

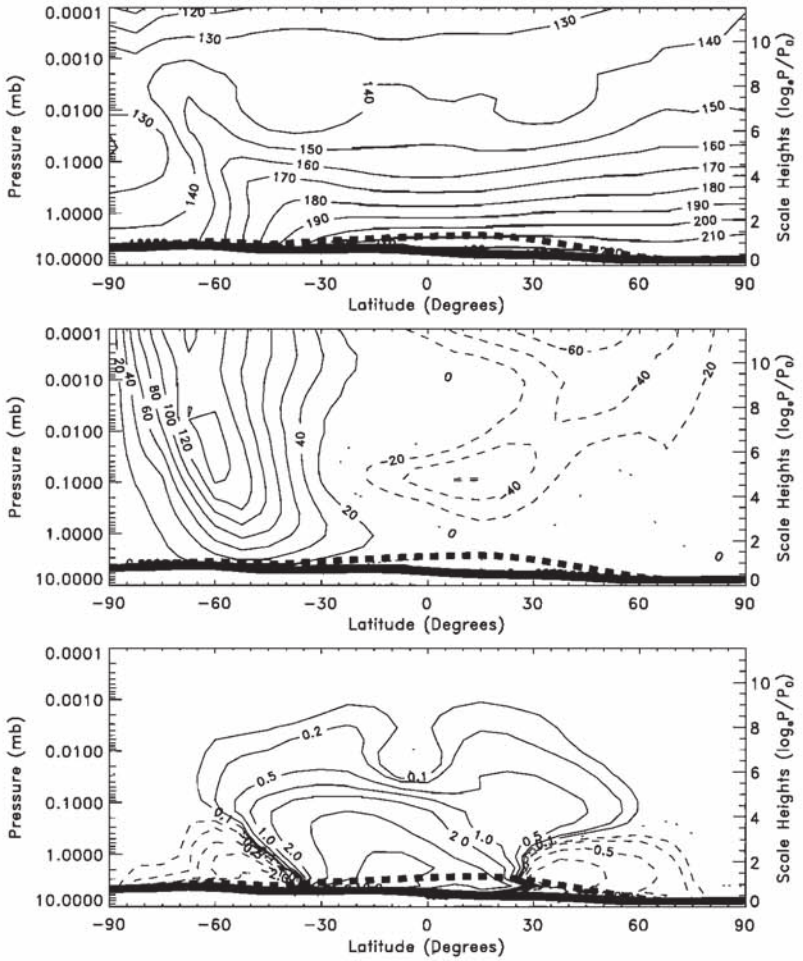

Figure 4. (top) Time and zonally averaged temperatures (K), (middle) zonal winds (m/s), and (bottom) mass stream function (10^8 kg/s for the 10 sol period centered around $L_s = 142°$. Thick solid line is the zonally averaged mean surface pressure; thick dashed line indicates the pressure level at which grid points begin to be eliminated from the zonal average because of topography.

$L_s = 0°$, we give the model enough time for the CO_2 cycle and dynamics to equilibrate. In the discussion that follows, we focus on the model results for the 83 sols beginning at $L_s = 142°$ and ending at $L_s = 187°$. For those simulations which assess the sensitivity of our standard model parameters, we warm start the model at $L_s = 120°$ from our standard simulation.

6. Global Patterns

The basic features of the general circulation at the time Pathfinder entered the atmosphere, as simulated by the MGCM, are shown in Figure 4. Overall, these are similar to those from our earlier version discussed by *Haberle et al.* [1997]. Westerlies prevail throughout the middle and high latitudes of the southern hemisphere, where the atmosphere is stably stratified with a pronounced tongue of warm air that tilts poleward with latitude. This latter feature is the classic signature of adiabatic warming associated with the descending branch of a large cross-equatorial Hadley circulation. The main difference between the present simulation and our earlier simulation is that the tropical middle atmosphere is warmer and the northern midlatitude westerlies are weaker. These differences are mostly due to the fact that in the present simulation, dust extends several scale heights higher in altitude than in the earlier simulation.

At the end of the Pathfinder mission, modeled global patterns had changed significantly (Figure 5). By $L_s = 180°$, the meteorological fields have become much more symmetric about the equator. Westerlies of comparable strength have developed in the midlatitudes of both hemispheres, as is reflected in the similarity of the equator-to-pole temperature gradients in each hemisphere. The Hadley circulation now consists of two cells with a common rising branch roughly centered on the equator, though the northern cell is now considerably stronger than the southern cell. At this season the wave-induced high-latitude Ferrel cells have comparable strength to the Hadley cells.

At the Pathfinder latitude, the simulated changes in the zonal mean zonal wind and temperature fields are minor, but the model indicates a transition in the zonal mean meridional winds from southerly at Pathfinder's arrival to northerly by end of mission. A similar transition occurs at the Pathfinder longitude. This change is associated with the southward migration of the rising branch of the Hadley circulation. There is some indication in the Pathfinder data for a similar shift in wind

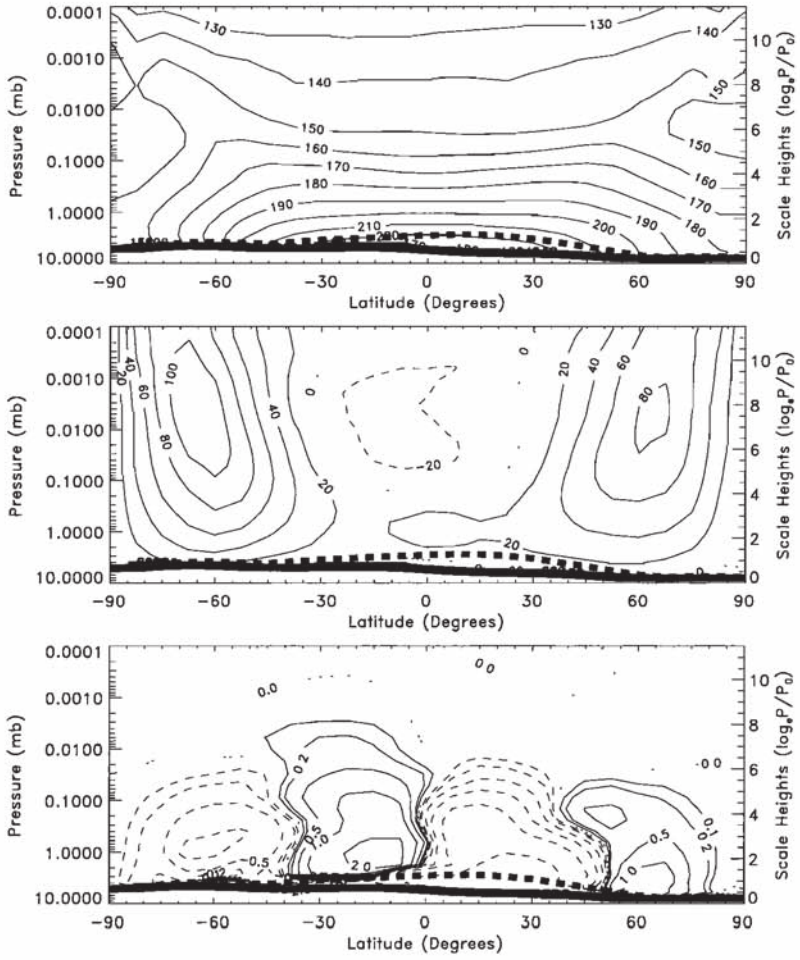

Figure 5. Same as in Figure 4, but for $L_s = 180°$.

directions near the end of the mission (not shown). It is worth pointing out that this is also the time of year that the winds at VL-1 transitioned from a slope controlled regime, to a Hadley controlled regime [*Murphy et al.*, 1990].

7. Entry Phase

To date, the analysis of the accelerometer data has provided atmospheric structure information from about 160 to 9 km above the ground [*Schofield et al.*, 1997; *Magalhaes et al.*, this issue]. We compare the results of these analyses with our nominal MGCM simulation in Figure 6.

The 10-sol composited temperature from the MGCM at 0336 hours (the output time closest to 0258 hours) agrees quite well with the entry data. The composited profile has about the same domain averaged lapse rate as the entry data, and it shows wavelike structure above the 0.1 mbar level. The main discrepancies are in the region above 0.1 mbar, where the MGCM profile is out of phase with the entry data, and in the region between 0.9 and 1.0 mbar, where the entry data show a pronounced inversion. The MGCM does predict an inversion, but it is much closer to the surface and is very shallow. While this latter feature is sensitive to our uncertain treatment of the stable boundary layer, it is not likely to be the reason the MGCM does not predict the elevated inversion seen in the entry profile.

Also shown in Figure 6 are each of the 10-sol 0336 hour profiles from which the composite was formed. Clearly, there are sol-to-sol variations due to dynamical processes that are not tied to the diurnal cycle. This sol-to-sol variability increases with altitude and can be as much as 70 K in the upper atmosphere. On several occasions these dynamical processes push temperatures below 100 K, which suggests that the minimum temperature recorded during Pathfinder's descent (92 K at about 10 scale heights) could be dynamically produced. *Schofield et al.* [1997] suggested that CO_2 ice clouds may form in this region. Thus dynamical processes may play an important role in their formation. However, we have less confidence in the model results at these high levels, since our radiation scheme does not yet include non-LTE effects in the infrared and since we are parameterizing gravity wave breaking with a simple Rayleigh friction scheme [see *Pollack et al.*, 1990]. Both these processes need better representation before firm conclusions can be drawn.

While the relative roles of dynamics and radiation in this part of the atmosphere need further study, there are several indications in MGCM simulations that both processes are important. In Figure 6 we also present the results of a purely one-dimensional (1-D) radiative-convective calculation based on the MGCM diabatic heating algorithms. The afternoon and morning profiles give some estimate of the role of radiative

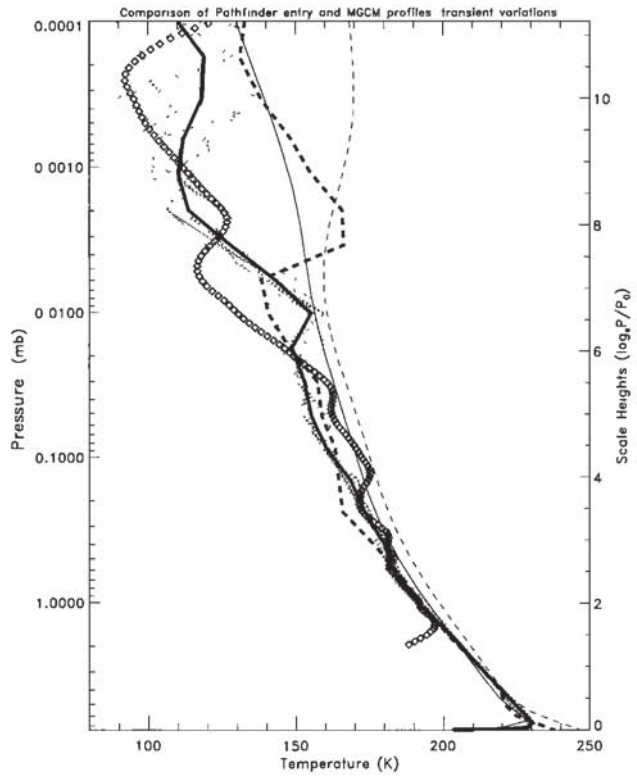

Figure 6. Temperature profiles from Pathfinder observations (open diamonds) and 10 sol averaged MGCM simulations: 0336 hour temperatures (thick solid line); 1536 hour temperatures (thick dashed line); each of the 10 sols used to form the 0336 hour average (thin dotted lines). The thin solid and dashed lines are from a 1-D radiative-convective simulation for 0336 (thin solid line) and 1536 (thin dashed line). The 10 sol composite is centered around $L_s = 142°$. A scale height is approximately 10 km.

heating in controlling daily temperature variations. Diurnal radiative heating and cooling clearly become significant above eight scale heights. Near the model top, temperatures vary by 40 K between 0336 and 1536 hours. Also, above five to six scale heights the 1-D profiles are considerably warmer than those from the full MGCM, which indicates the dynamical processes are cooling this region of the atmosphere.

In Figure 7 we compare MGCM simulations with the Pathfinder entry data for conditions in which we (1) eliminated the non-LTE solar heating correction factor, (2) ran the model with daily-averaged solar insolation to eliminate the tides, and (3) ran the model with the dust confined to much lower altitudes. There are several points worth making from these simulations.

First, the simulation without the non-LTE solar heating rate correction shows daytime temperatures in the 80–100 km region that are on average ~20 K warmer than when the correction is included (not shown in Figure 7). This is not surprising, since non-LTE effects tend to reduce solar heating rates in the upper atmosphere [*Lopez-Valverde et al.*, 1998]. At night, however, temperatures are less affected because of the short radiative relaxation time, so that the composited 0336 hour temperature profile for this case is not significantly different from that in the nominal run. However, until we can fully assess how non-LTE effects change the model infrared cooling rates, we cannot be certain that nighttime temperatures will be similar to the nominal values given in Figure 6.

It is also interesting from Figure 7 that the non-LTE effect is not just limited to the upper atmosphere. Without the solar correction, temperatures are uniformly warmer (~5 K) in the 0336 hour profile almost all the way to the surface. It is generally assumed that the upper atmosphere responds to forcing from the lower atmosphere and that there is no feedback to the lower atmosphere [e.g., *Bougher et al.*, 1993]. However, Figure 7 suggests the interaction goes both ways.

Second, as mentioned above, atmospheric motions tend to cool the upper atmosphere at the Pathfinder location and season. The type of atmospheric motions involved needs further study, but thermal tides appear to play an important role. This is indicated from the profile in Figure 7 that was generated without diurnal forcing. Above eight scale heights, temperatures are 30–50 K warmer than when the full diurnal cycle is included. This indicates that the tides are not only imposing a wavelike structure in the profile, but are changing the mean temperature structure as well. This latter result implies that it is the wave-induced tidal heat flux divergences that are responsible for cooling the upper atmosphere. That the tides have a significant impact on the upper atmosphere zonal mean flow has been suggested by several investigators [*Hamilton*, 1982; *Zurek*, 1986; *Zurek and Haberle*, 1988].

Finally, we also show in Figure 7 the results from a simulation in which the dust is confined to the lower atmosphere

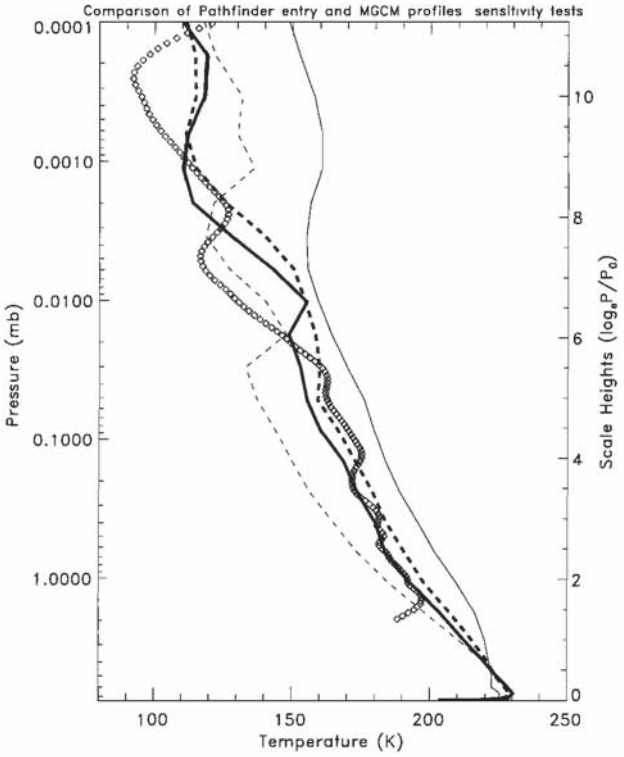

Figure 7. Temperature profiles from Pathfinder observations (open diamonds) and 10 sol averaged 0336 hour MGCM simulations for the standard run (thick solid line); a run without the non-LTE correction factor (thick dashed line); a run forced with daily averaged insolation, i.e., no diurnal cycle (thin solid line); and a run with dust confined to the lowest several scale heights (thin dashed line).

($\nu = 0.1$ in Figure 2). For this profile the dust mixing ratio falls to 50% of its surface value at the 1 mbar level (approximately two scale heights) as compared to the 0.02 mbar level (approximately six scale heights) in our nominal simulation ($\nu = 0.003$). Much cooler temperatures prevail in the lower atmosphere for this experiment, which suggests that the dust was distributed deeply in the Martian atmosphere at the time Pathfinder landed.

Though there was no direct measurement of wind during Pathfinder's entry and descent, trajectory reconstruction calculations indicate that the lander's horizontal impact velocity was ~6 m/s toward the north-northwest [*Golembek et al.*, this issue]. This implies that near-surface winds were light and out of the southeast at the time of touchdown. The MGCM 10-sol composited 0336 hour entry winds are shown in Figure 8. Near-surface simulated winds are light and easterly. In the lowest kilometer they are generally from the northeast rather than southeast. Aloft, the winds reverse and are out of the west but remain fairly light.

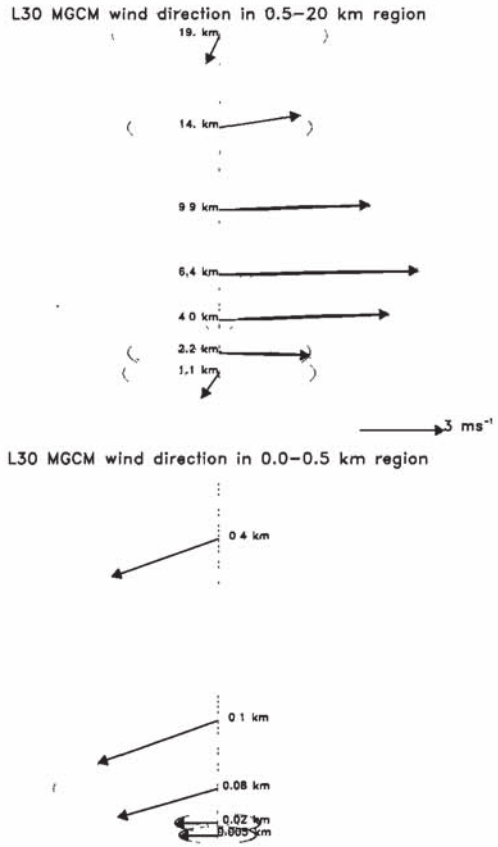

Figure 8. Ten-sol composited MGCM wind vectors in the lower atmosphere corresponding to the entry time and season of the Pathfinder landing. Dotted ellipses give an oblique view of a compass rose for each layer. Vectors point in the direction the wind is blowing toward. A reference 3 m/s wind vector is given in the middle of the figure.

8. Landed Phase

We now compare the MGCM with the landed measurements. Figure 9 shows composited temperature, pressure, and wind direction for the primary mission (the first 30 sols). The temperature data are from the top mast thermocouple at 1.27 m above the ground, binned into 51 evenly spaced times of day.

Pathfinder's daily temperature cycle was quite repeatable with highs near 260 K and lows near 200 K. MGCM 5 m temperatures are also quite repetitive at this season and closely match Pathfinder's nighttime temperatures. During the day, however, they are consistently cooler than Pathfinder's. This is due to the different heights the model and data refer to, as well as the fact that the MGCM employs an instantaneous convective adjustment to the temperature profile, which overestimates the vertical turbulent heat flux [*Haberle et al.*, 1997].

We performed an experiment in which we relaxed the convective adjustment in the lowest kilometer of the atmosphere. This was done by multiplying the convective adjustment tendencies by a factor which decreased monotonically from one at and above 1 km, to zero at the surface. (The model has numerical problems with the convective adjustment turned off entirely.) The results are shown in Figure 10.

The simulated daytime 5 m temperatures are about 5 K warmer and maximize about an hour earlier than in the run with full convective adjustment. These changes in the amplitude and phase give better agreement with the data and suggest that near the surface, the atmosphere is highly unstable during the day. This is also indicated in the MET mast profile measurements, which show an ~8 K daytime temperature difference between the top and bottom thermocouples which are separated by only 0.75 m [see *Schofield et al.*, 1997, Figure 5]. This lapse rate greatly exceeds the adiabatic lapse rate (~0.005 K/m) resulting from convective adjustment by many orders of magnitude.

Returning to Figure 9, we can see that the MGCM diurnal surface pressure variation is not as great as that seen at the Pathfinder site. While the MGCM does reasonably well in simulating the phase of the diurnal variation, it underestimates the morning maximum and afternoon minimum. This deficiency is more clearly illustrated in Figure 11, which gives the amplitude and phase of the diurnal and semidiurnal tide. For both components the MGCM underestimates tidal amplitudes by as much as a factor of 2. Simulated phases are in better agreement with the data, particularly for the semidiurnal tide.

It should be pointed out here that the amplitudes and phases of the Pathfinder tides shown in Figure 11 differ from those reported by *Schofield et al.* [1997]. The differences are due to reprocessing the pressure data with an improved temperature calibration (see the appendix). The amplitude of the diurnal tide is now 2–3 times greater than in the preliminary analysis, and the phase is steadier and closer to that expected for the classical tide (0600 hours). The semidiurnal component is less affected by the new calibration, though its amplitude has increased slightly and its phase has advanced slightly.

Two other Mars GCM groups have been successful in simulating the Pathfinder diurnal tide: the Oxford group in the United Kingdom [*Lewis*, 1998] and the Laboratoire de Météorologie Dynamique (LMD) group in Paris (F. Forget, personal communication, 1998). On the other hand, our model and the model of *Wilson and Hamilton* [1996] underestimate Pathfinder's diurnal tidal amplitude. Thus, at present, tidal signatures are quite model dependent, and until the reasons for the differences are understood, the performance of this aspect of GCMs will be difficult to interpret.

Figure 11 also shows the tides observed at VL-1 for the 20 sols that overlapped with the season of the Pathfinder primary mission. The average amplitude of the diurnal tide at the

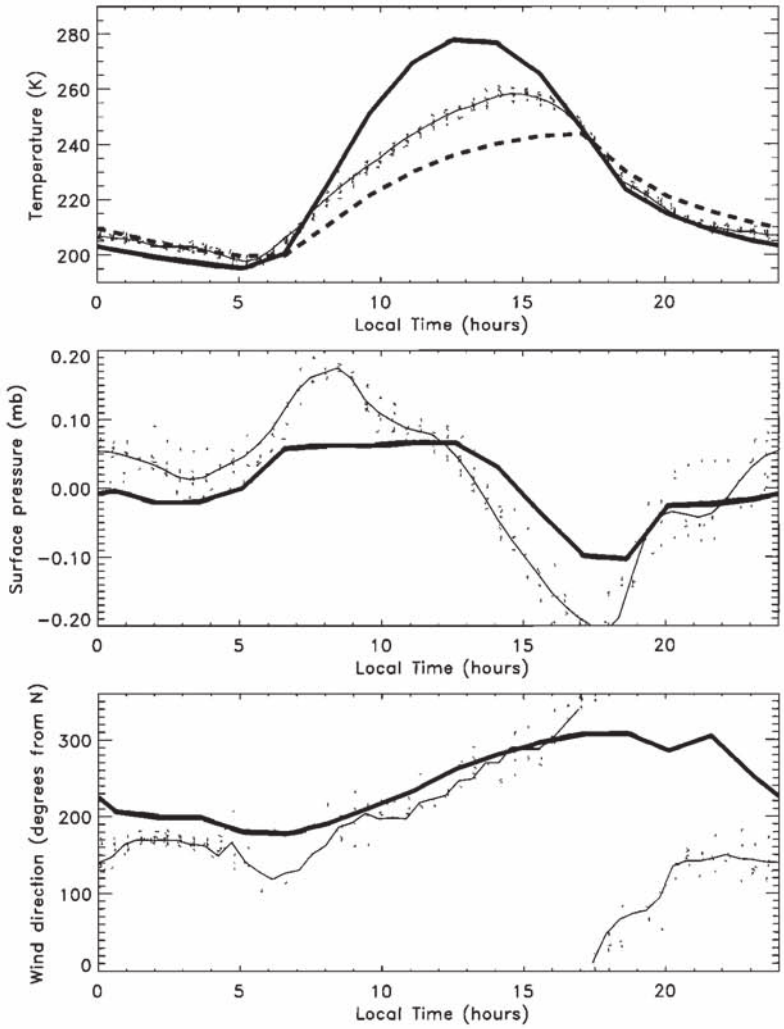

Figure 9. Composited daily variation of the meteorological fields from the Pathfinder MET experiment and the MGCM. The compositing is based on the 30 sol primary mission. The data are binned into 51 equally spaced times of day; the model results are binned into 16 equally spaced times of day (the output frequency of the MGCM). The thin solid line is drawn through the mean value of each bin in the Pathfinder data set. The dots are session averages of the data. (top) MGCM ground temperature (thick solid line) and 5 m air temperature (dashed line). Pathfinder data are for the top mast thermocouple (1.27 m above ground level). (middle) MGCM surface pressure (thick solid line). The time mean has been removed. (bottom) MGCM wind direction (thick solid line).

Pathfinder site is about 50% greater than at VL-1 for the same period (0.018 at Pathfinder compared to 0.012 at VL-1). It is possible that the new calibration is overestimating the temperature correction and that this is giving rise to the rather large tidal amplitudes. On the other hand, there are large variations in tidal amplitudes at VL-1 that are not present in the Pathfinder data, which may be due to interference effects that are not occurring in the same manner at the Pathfinder site. In particular, the VL-1 tidal amplitudes increase then decrease, while at the same time the phase advances, particularly for the diurnal component. On several occasions, VL-1 diurnal amplitudes are actually larger than those seen by Pathfinder.

The variations in VL-1 tides are not well understood. However, *Tillman* [1988] has suggested they are annually synchronized events that arise from the interference effects of eastward and westward traveling tidal modes. In this case, the eastward mode is a resonantly enhanced Kelvin wave with a period slightly less than a sol (which explains the advancing phase). No such events were seen by Pathfinder, i.e., there were no abrupt increases in tidal amplitudes and very little variation in tidal phases. These results indicate that if interference is contributing to Pathfinder's large diurnal tidal amplitude, then it is a quasi-stationary feature (the eastward mode must have a period at or very close to a sol) and Pathfinder must be at a location where the interference is constructive.

Of course, it is possible that variations did occur on those sols for which there were not enough data to define the tide, such as a possible transient event on the very first sol [see *Schofield et al.*, 1997]. However, the Viking observations suggest the transient events span a period of 5–10 sols, which means that if they did occur during Pathfinder's primary mission, some signature would have been detected even though the coverage was not ideal. Thus it is not likely there were any transient events during the primary mission after sol 1.

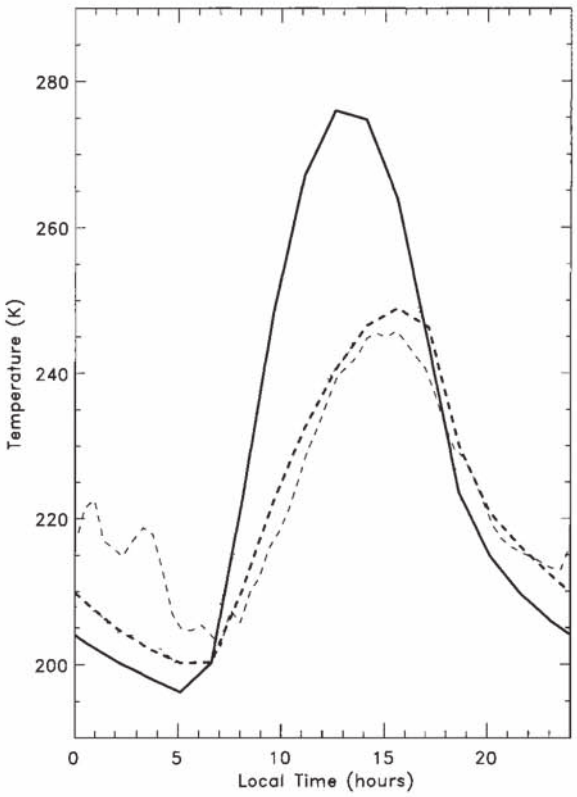

Figure 10. MGCM temperatures for a run with reduced convective adjustment (see text): ground temperature (thick solid line), 5 m air temperature (thick dashed line). The thin dotted line is a linear extrapolation (in log space) of Pathfinder's bottom two thermocouple measurements to the 5 m level. The thin dashed line is a similar extrapolation using the top two thermocouple measurements.

At this time, wind comparisons are limited to direction only, since laboratory work is needed to properly calibrate the wind sensor data for wind speed. In Figures 9 and 12, we compare MGCM wind directions with those inferred from Pathfinder based on azimuthal variations of wind sensor overheats. While surface winds are the most sensitive meteorological parameter to local effects (and are therefore less suited for direct comparison with a GCM), there are several features in the Pathfinder data that may be representative of regional-scale wind systems, namely, the winds appear to be light (<10 m/s based on the wind sock experiment; see *Smith et al.* [1997]), and they rotate clockwise with time. MGCM winds have similar features. They rotate clockwise at about the same rate during the period 0600–1500, and the wind speeds are generally light (<12 m/s; see Figure 12).

The MGCM wind speeds shown in Figure 12 exhibit a behavior similar to that observed by VL-1 for this season [*Murphy et al.*, 1990]. Winds are calm at night and are strongest during the afternoon. In the model, winds tend to increase with height, so that during the day, turbulence mixes the relatively stronger winds aloft to the surface. At night the near-surface atmosphere decouples from the upper levels as the temperature profile stabilizes. This pattern is roughly consistent with the preliminary wind sock results, but the strongest MGCM winds are occurring later in the day (~1600) than what has been inferred from the wind socks (~1200). It will be interesting to see what pattern emerges from the Pathfinder wind sensor data.

Simulated surface heat and momentum fluxes are shown in Figure 13. The fluxes are very small at night, when the atmosphere is stable, but increase substantially during the day, when the atmosphere is unstable. Maximum simulated surface stress is ~15 mPa in the early afternoon. This peak value is well below the threshold value for lifting dust into the atmosphere by saltation (~35 mPa [*Greeley and Iversen*, 1985]). To the extent that these values are correct, it implies that the large-scale circulation is incapable of lifting dust at this location and season. This further implies that the atmospheric dust loading observed by Pathfinder [see *Smith et al.*, 1997] is either brought in from elsewhere on the planet and/or it is locally derived by small-scale circulation features such as the "dust devils" that were observed by Pathfinder and Viking [*Schofield et al.*, 1997; *Ryan and Lucich*, 1983].

The peak heat fluxes shown in Figure 13 are similar those estimated for the VL-1 site earlier in the season [*Sutton et al.*, 1978]. This is due to the use of the same surface roughness (1 cm), a similar surface layer formulation, and the fact that the GCM is producing similar values of the daytime air-to-ground temperature difference (~25 K). However, if the simulated air temperature is too cold due to convective adjustment, then the simulated heat fluxes will be too large.

The extended mission covered the period from sol 30 to sol 83, when the last science data packets were returned to Earth. In order to extend battery lifetime, science data collection during this part of the mission was limited mostly to daytime observations (~1000–1500 hours). There were, however, 4 sols for which continuous 4 s sampling was permitted for an entire sol. These occurred on sols 32, 38, 55, and 68. Only for these sols was it possible to define the diurnal cycle during the extended mission. Table 2 gives tidal amplitudes and phases for these sols.

For the most part, the amplitude and phase of the tides computed for these sols do not differ significantly from those of the primary mission. MGCM simulated tidal amplitudes and phases for this period (not shown) also do not change much from their values during the primary mission. Thus their amplitudes remain considerably less than observed.

A comparison of the simulated and observed surface pressure for the entire mission is shown in Figure 14. Simulated daily average surface pressures show an upward trend during the extended mission, as is also indicated in the data. However, it is not possible to construct meaningful daily averages of the data. Therefore, in Figure 14 we also compare modeled and observed surface pressures at 1130 hours. This time of day was frequently sampled by Pathfinder. In this comparison, the MGCM agrees exceptionally well with the data. However, it should be noted that our good agreement with the data is mostly due to the fact that our polar cap properties were "tuned" to fit the VL-1 pressure data, which is very similar to Pathfinder's data. The upward trend in the pressure data is due to the sublimation of the south polar cap, which has begun its annual retreat.

9. Discussion

9.1. Distribution of Dust

Our simulations of Pathfinder's ASI/MET data suggest that the dust observed at the site is deeply distributed throughout the atmosphere. Our simulated entry profile is too cold if the

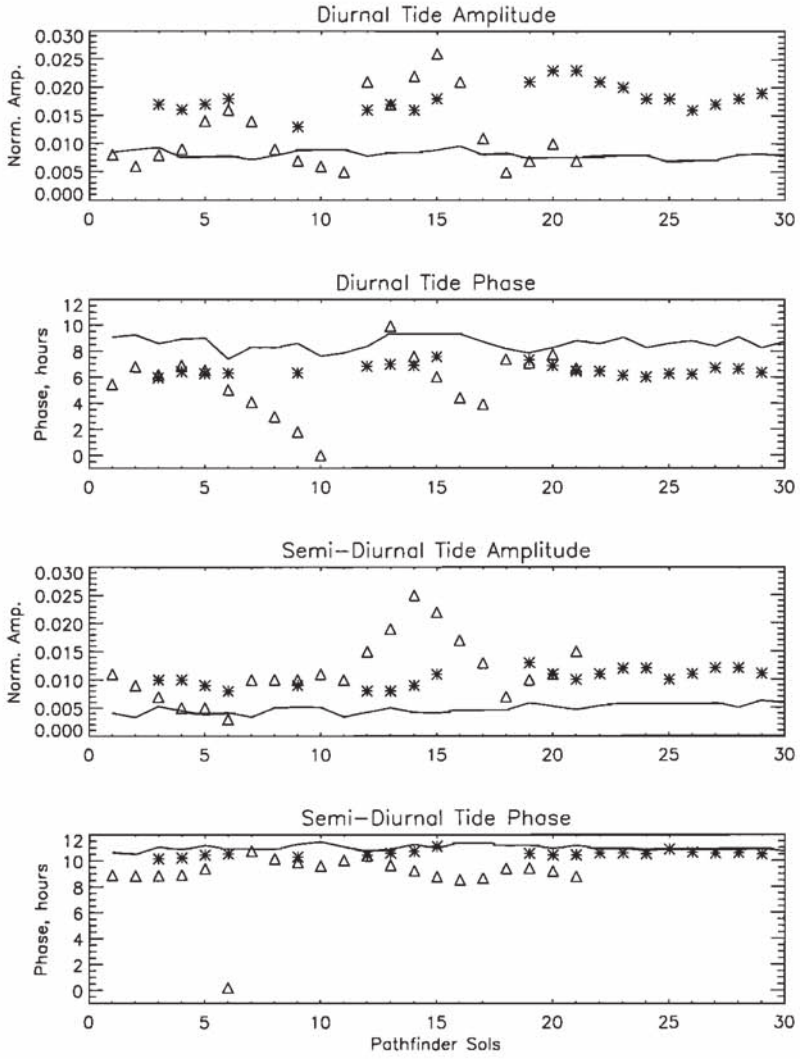

Figure 11. Surface pressure tidal amplitudes and phases from the Pathfinder data (stars), Year 1 VL-1 data (open triangles), and the MGCM (thin solid line). Note gaps in the data.

dust is not present at least up to five or six scale heights. Deeply distributed dust is also indicated by Pathfinder's large semidiurnal tidal pressure component. There are, of course, uncertainties in the pressure calibration. However, they have less effect on the semidiurnal tide than the diurnal tide. Therefore, if the dust at the Pathfinder site is distributed as deeply as our simulations imply, then it is also likely to be distributed over large horizontal distances as well.

If we assume, for example, that the dust particles have effective radii of ~1 μm, then at 50 km, the time it takes to fall to the surface is about 10 sols [*Murphy et al.*, 1990]. Taking a rather conservative estimate of 10 m/s for the average zonal wind speed between the surface and 50 km, then in 10 sols a 1 μm size particle will travel $\sim 10^7$ m, which is about halfway around the planet at Pathfinder's latitude.

Yet a deep global dust haze is not consistent with the Earth-based microwave observations taken just before (June 26, 1997) and just after (July 14, 1997) Pathfinder landed (T. Clancy, unpublished data, 1997). Those data indicate a slight warming trend from June to July, but in both observations, temperatures remain considerably (~20 K) cooler than Pathfinder's entry profile between 0 and 40 km.

One possible explanation for these differences is that the microwave data are disk-averaged while the Pathfinder entry profile pertains to a single site. We used the MGCM temperature field to compute a disk-averaged temperature profile using the Earth-Mars viewing geometry appropriate to the Pathfinder landing date. This profile is compared to the Pathfinder entry profile (both simulated and observed) in Figure 15.

In the region of interest (10–50 km) there is very little difference between the disk-averaged profile and the entry profile. The only significant differences occur above 50 km, where the radiative and dynamical processes discussed above can cause significant diurnal variations, and below 10 km, where spatial variations due to local time of day effects become increasingly pronounced and where the disk-averaged profile is based on a smaller (horizontal) fraction of the atmosphere because of large variations in surface topography.

The reason for the small differences between the simulated disk-averaged and simulated entry profile is partly coincidence (the simulated profile happens to be representative of the disk average) and partly due to the fact that MGCM temperatures do not vary that much horizontally or in local time, at least for this season. This is an important point. The disk-averaged

profile is heavily weighted by temperatures around the sub-Earth point, which for the profile shown in Figure 15 is located at 26°N and 120°W with a local time of 1000 hours. We have projected the MGCM temperature field onto a disk centered at this sub-Earth point and show that field for the 0.4 mbar level (~28 km) in Figure 16. Within 30° of the sub-Earth point where the weighting is largest, temperature variations are ~10 K. Cooler temperatures can be seen at high southern latitudes, but they are so close to the edge of the disk, they have very little effect on the disk average. We conclude that if temperature variations in the Martian atmosphere are similar to those simulated by the MGCM, then the difference between the Pathfinder entry profile and the June/July microwave profiles cannot be attributed to the disk-averaging nature of the microwave data.

Another possibility is that there are spatial variations in the dust which can account for the difference. We have argued for a global haze in this paper, but it does not need to be spatially uniform. If the dust is concentrated in low-lying areas, for example, then these would be warmer than elsewhere. In this situation the disk-averaged temperature would be lower than those in low-lying regions. We have explored this possibility with the MGCM in a run in which the dust optical depth at the Pathfinder grid point was as given in Figure 3, but elsewhere it was proportional to the square of the surface pressure. While the simulated disk-averaged temperatures in the lower atmosphere of this run do cool, the change is only several Kelvins. This is because even though dust is reduced over upland regions, there is still enough to keep temperatures relatively warm compared to clear conditions. Our modeling of the radiative properties of the dust indicates that temperatures are very sensitive to modest amounts of dust. Thus, to substantially reduce the disk-averaged temperature, the upland regions would have to be virtually clear of dust. We cannot rule out this possibility but believe it unlikely, since it would not yield a global dust haze.

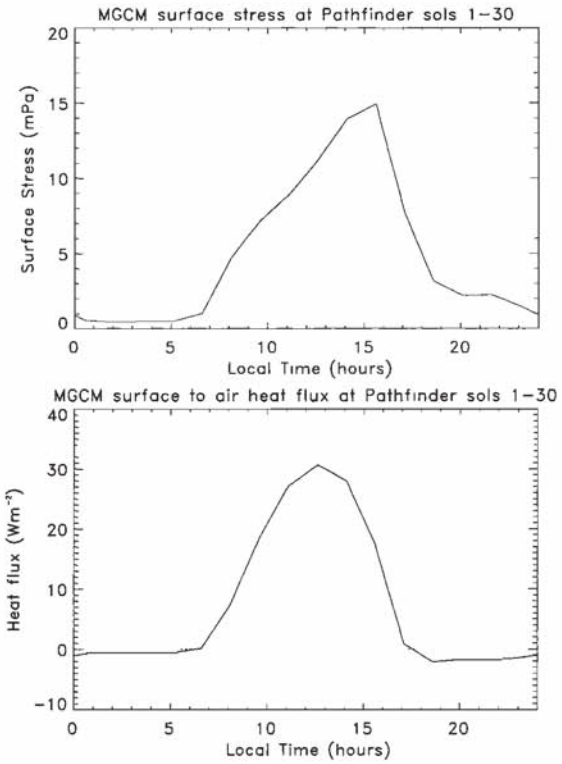

Figure 13. Thirty-sol composited MGCM (top) surface stress and (bottom) surface heat flux.

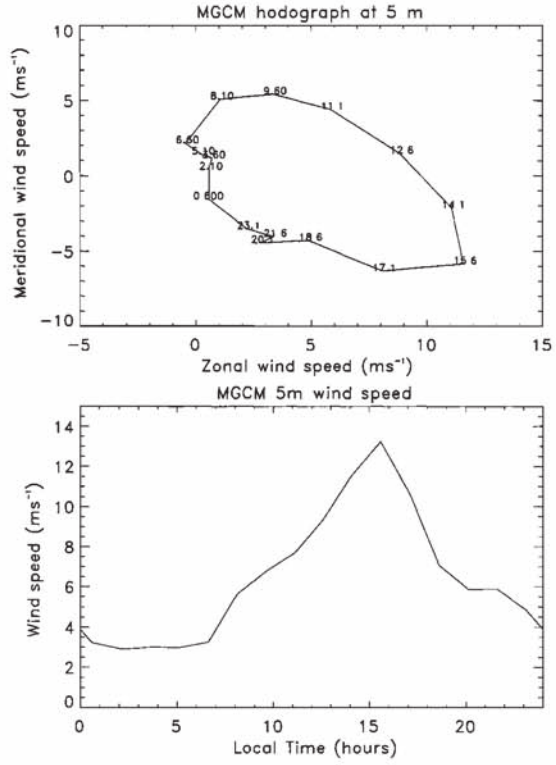

Figure 12. Thirty-sol composited MGCM near-surface winds displayed (top) in hodograph form and (bottom) as wind speed only. Numbers in the hodograph refer to the local time of day a given point on the curve refers to.

Nevertheless, the possibility for spatial variations in atmospheric dust needs further study. *Wilson and Hamilton* [1996] have shown that during early northern summer the circulation organizes itself in such a way as to enhance the concentration of dust over upland regions relative to lowland regions. This is opposite of what is required to explain the difference between the disk-averaged microwave observations and the Pathfinder entry profile. But at that season (early northern summer), enhanced dust over upland regions does reduce the response of the eastward Kelvin mode whose amplitude is otherwise too large in simulations with horizontally uniform dust loadings [*Bridger and Murphy*, 1998]. Wilson and Hamilton argue that by reducing the Kelvin mode response, enhanced dust concentrations over upland regions give much better agreement with the diurnal tidal amplitudes observed at VL-1 at this season.

Table 2. Tidal Data for the Extended Mission

Sol	L_s	Diurnal Amplitude	Diurnal Phase	Semidiurnal Amplitude	Semidiurnal Phase
32	160	0.021	7.07	0.010	11.27
38	163	0.022	7.10	0.010	10.89
55	172	0.022	6.60	0.013	11.27
68	180	0.022	6.63	0.012	11.13

Phases are given in decimal hours.

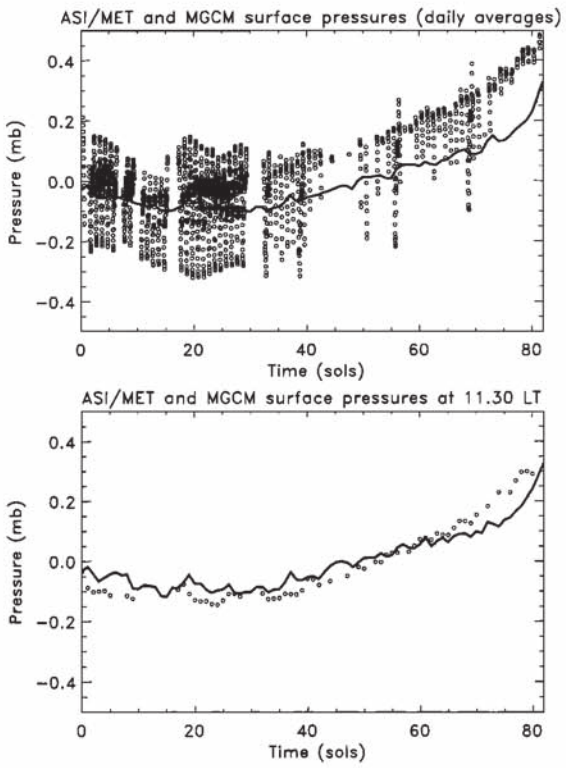

Figure 14. Surface pressure trends from Pathfinder observations (open circles) and MGCM results (solid line). Time means have been removed. Top panel shows all of Pathfinder's binned data. The MGCM curve is based on daily averages. Bottom panel shows results for 1130 only.

Our simulations have the opposite problem. Our simulated diurnal tidal amplitudes at the Pathfinder site are significantly smaller than observed. Tidal amplitudes can be increased by directly boosting the tidal forcing or by exciting eastward modes which constructively interfere at the Pathfinder site. It is difficult to conceive of a way to boost tidal forcing much beyond our present calculations without increasing the global dust loading. This leaves interference effects as the most viable option. It is possible that our small tidal amplitudes are due to modes which are destructively interfering.

In Figure 17 we show the longitudinal dependence of our standard model's 30-sol average of the diurnal and semidiurnal tidal amplitudes at the Pathfinder latitude. Around this latitude circle, both components vary by factors of 2–3, which clearly indicates interference is occurring. The interference pattern is particularly striking for the semidiurnal component which has a very well defined wave-4 structure, as is expected for eastward and westward propagating wave-2 modes. At the Pathfinder longitude (~33°W), the semi-diurnal component is near a minimum, and the diurnal component is relatively small as well. However, at no longitude does the diurnal component reach Pathfinder values, and only at a few longitudes does the semidiurnal component reach Pathfinder values. Thus other factors must be important. For horizontally uniform dust loadings the MGCM Kelvin mode response is declining during the Pathfinder season [*Bridger and Murphy*, 1998]. In the future we plan to explore what spatial patterns of dust, if any, generate interference effects which increase the diurnal tidal response at the Pathfinder site.

9.2. Pathfinder/VL-1 Entry Profile Comparison

A comparison of the Pathfinder and VL-1 entry profiles is shown in Figure 18. In the lower atmosphere the Pathfinder and VL-1 entry profiles are similar, whereas in the upper atmosphere the Pathfinder temperatures are generally cooler than those in the VL-1 profile. The difference can be as much as 40 K at the 200 nbar level (~10 scale heights). Given that Pathfinder and VL-1 are close in proximity to each other, these upper atmosphere differences are likely due to several possibilities.

First is season. Pathfinder landed in midnorthern summer (L_s = 142°), whereas VL-1 landed in early northern summer (L_s = 96°). However, the change in the available insolation at the top of the atmosphere at the Pathfinder latitude is only at the several percent level. Thus the change in direct radiative forcing is relatively small. A second possibility is local time of day effects. Pathfinder landed at 0258 hours, whereas VL-1 landed at 1615. If local time of day effects are important, then the issue is whether they arise due to radiative and/or dynamical effects. Our simulations for the Pathfinder site indicate that both are important, and this is likely to be the case at VL-1 as well. However, to properly assess these effects, an improved treatment of non-LTE effects at both solar and infrared wavelengths is needed. Also needed is a thorough study of the role gravity waves and gravity wave breaking play in controlling the structure of the upper atmosphere. We plan to investigate these in future studies as well.

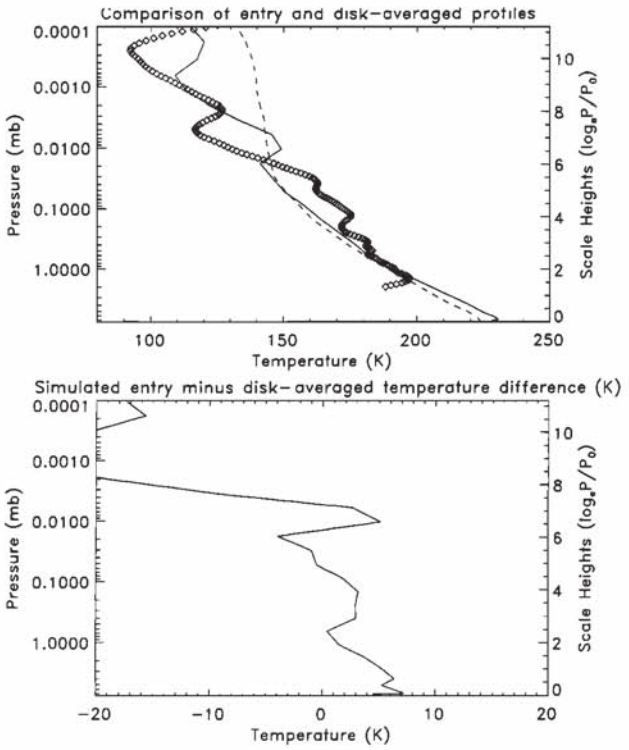

Figure 15. (top) Comparison of Pathfinder entry data (open diamonds) with the MGCM 10 sol averaged 0336 hour profile (solid line), and the MGCM disk-averaged profile (dashed line). The sub-Earth point for the disk average is 26°N, 120°W at 1000 hours. The disk average is a weighted average based on the projected area of the planet as seen from Earth. (bottom) Difference between the entry profile and MGCM simulated disk-averaged profile.

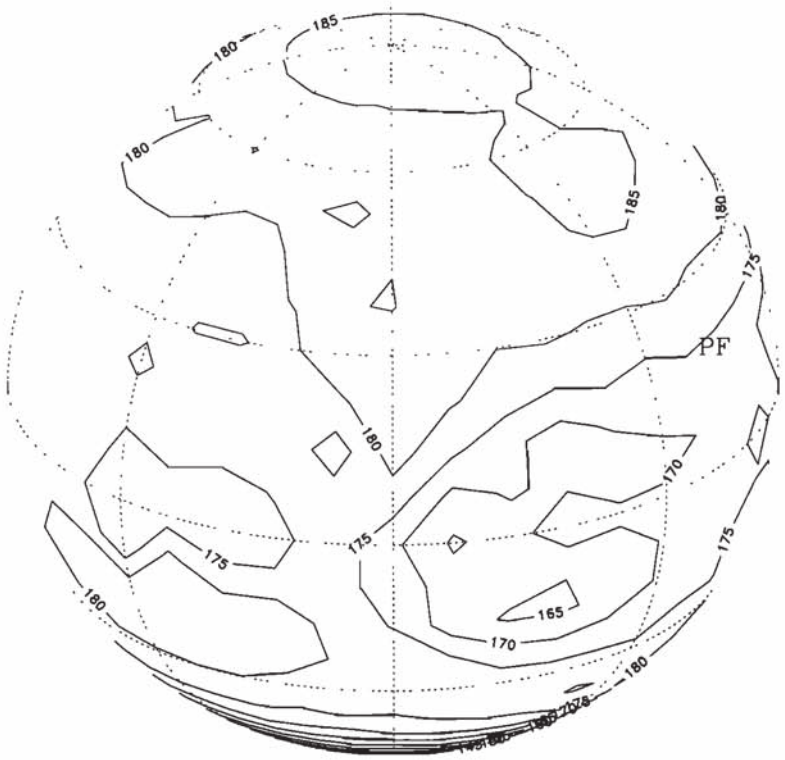

Figure 16. MGCM temperature field at the 0.4 mbar level (~30 km) projected onto a sphere centered on 26°N, 120°W at 1000 local time (the sub-Earth point for the disk-averaged temperature profile of Figure 14). The point marked PF corresponds to the Pathfinder latitude and longitude.

9.3. Low-Level Inversion

A final point worth discussing is the elevated inversion between 10 and 16 km in the Pathfinder entry profile. The presence of such a deep elevated inversion was a surprise. Evidently, the MGS Radio Science Experiment is also finding deep early morning inversions at some locations (L. Tyler, personal communication, 1998). Thus these inversions may be robust features of the nighttime atmosphere. One-dimensional

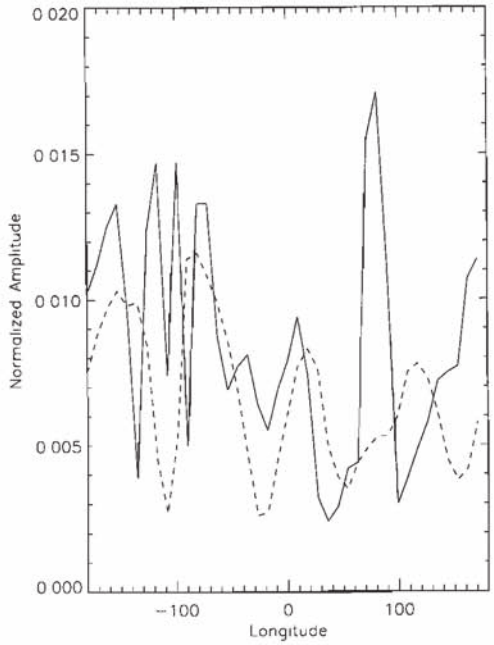

Figure 17. Longitudinal variation of the normalized diurnal (solid line) and semidiurnal (dashed line) tidal amplitudes at the Pathfinder latitude.

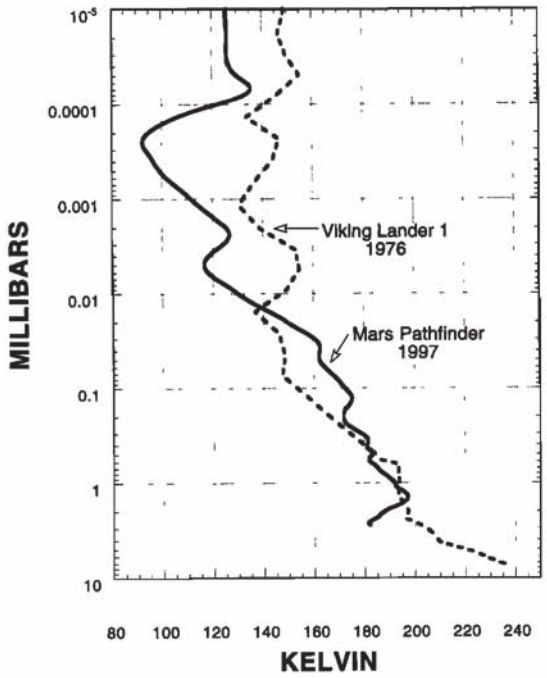

Figure 18. Pathfinder and VL-1 entry profiles.

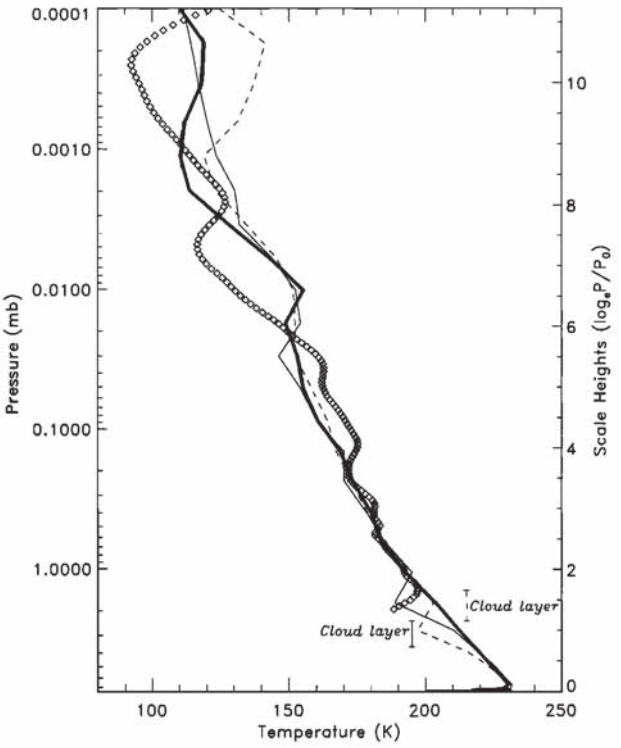

Figure 19. Same as in Figures 6 and 7 but for MGCM simulations in which a $\tau = 0.5$ water ice cloud is prescribed at two different altitudes: between 2.4 and 3.6 mbar (thin solid line) and between 1.4 and 2.4 mbar (thin dashed line). The profile from our standard run (thick solid line) is shown for comparison.

radiative convective models do not simulate nocturnal inversions this deep and strong [e.g., *Gierasch and Goody*, 1968]. *Schofield et al.* [1997] suggested the possibility that thermal emission from cloud tops could play a role, since early morning clouds were observed by the Pathfinder imager [*Smith et al.*, 1997]. Furthermore, the calculations of *Flasar and Goody* [1976] show that the radiative effects of water ice clouds can have a significant effect on the thermal structure of the nighttime atmosphere.

The MGCM has algorithms to simulate the radiative effects of a water ice cloud. At solar wavelengths, water ice clouds are assumed to be pure scatterers and therefore simply alter the surface albedo [see *Pollack et al.*, 1981]. In the infrared the clouds alter thermal fluxes by changing layer emissivities [see *Pollack et al.*, 1990]. As is the case for dust, ice cloud emissivities are computed off-line from a Delta-Eddington code for the spectral regions inside and outside the 15 μm CO_2 band. The single scattering properties are computed from Mie theory assuming a modified-gamma size distribution extending from 0.5 to 10 μm with a mean particle size of 2 μm (radius).

To test the *Schofield et al.* [1997] suggestion, we ran the MGCM with a prescribed water ice cloud visible optical depth of 0.5 (~0.2 in the infrared). Based on recent microphysical calculations of *Colaprete et al.* [this issue] for the Pathfinder site, this is a plausible value. However, it may not be consistent with Pathfinder's camera observations [*Smith et al.*, 1997]. In any case, the cloud was assumed to exist only at night and extended between −7.5° and +37.5° latitude. In one simulation the cloud was bounded between 2.4 and 3.6 mbar (~7–11 km); in another it was bounded between 1.4 and 2.4 mbar (~11–16 km). The results are shown in Figure 19.

In both cases, enhanced cloud top thermal emission produces an inversion. The strength of the simulated inversions is less than observed, and they do not occur at precisely the same altitude as observed. The former may indicate that the cloud is more optically thick than assumed or that it has a different particle size distribution than assumed; the latter, however, is simply an artifact of our layer discretization. We believe these results demonstrate that water ice cloud cooling is a plausible mechanism for generating the observed elevated inversion. More detailed microphysical modeling is required to determine why a cloud would form in this region and what particle sizes it would have, as is more detailed radiative transfer modeling to more accurately assess their radiative effects.

10. Conclusions

In the lower atmosphere (less than five or six scale heights), radiative processes are the dominant influence on Pathfinder's temperature structure. In particular, it is very difficult to explain Pathfinder entry temperatures without invoking deeply distributed dust. The dust allows the atmosphere to absorb solar radiation and warm the atmosphere, which is otherwise too cold without it. Our simulations suggest that the dust is present up to five or six scale heights. This, in turn, implies that dust is also distributed over large horizontal scales, which is supported by Pathfinder's large observed surface pressure tidal amplitudes.

In addition to deeply distributed dust, our simulations indicate that nocturnal water ice clouds may also exert some radiative control on the lower atmosphere at night. We are able to simulate the observed low-level inversion with a 4–5 km thick ice cloud of optical depth 0.5.

Above five to six scale heights, dynamical processes exert an increasingly important role on the temperature structure. Pathfinder's cool mesosphere is not well simulated with models that do not include dynamics. Of the myriad possibilities, vertically propagating tides appear to be the most important, though a thorough assessment of the role of gravity waves needs to be made.

To simulate Pathfinder's near-surface air temperatures, we require a relatively low surface albedo (0.16), a moderately high soil thermal inertia (336 SI), and relaxation of convective adjustment. The soil properties set the amplitude and mean of the daily temperature variation, while relaxation of convective adjustment weakens the efficiency of turbulent mixing which gives better agreement with the phase. The latter indicates that the daytime near-surface Martian atmosphere is highly unstable.

Tidal pressure amplitudes at the Pathfinder site are not well simulated by the model. Both diurnal and semidiurnal components are underestimated. Simulated phases are in better agreement with Pathfinder data, particularly for the semidiurnal component. The reason for the amplitude discrepancy is uncertain; it may be due to inaccuracies in the pressure calibration or to interference effects between eastward and westward propagating tidal modes that are not captured by the MGCM.

Comparison with Pathfinder wind data is presently limited to direction, though some constraints on wind speed come from the wind sock experiment. In this regard, the MGCM is able to simulate the predominantly daily clockwise rotation of the wind vector but may be several hours late on the time of day

that maximum winds occur. However, given the strong control of winds by local effects, a more detailed comparison is not that meaningful.

Overall, the MGCM does reasonably well in simulating the Pathfinder data, including the upward seasonal trend in surface pressure. Its most notable deficiency is the weak surface pressure tidal amplitudes. Hopefully, future work will elucidate what mechanisms are involved, so that we can further improve the model and its utility for Mars weather and climate studies.

Appendix

The calibration of the ASI/MET pressure sensor used by *Schofield et al.* [1997] has been revised significantly for this paper. The Tavis pressure sensors used by ASI/MET are sensitive to temperature and must be calibrated to correct for this dependence. During prelaunch calibration, both the flight and flight spare pressure sensors were inadvertently exposed to temperatures 30 K below their design limits. This produced changes in sensor offset of several tenths of a millibar and increased the variation of offset with temperature by a factor of 7 relative to the original calibration. These changes were not noticed until spacecraft thermal vacuum testing, and by the time they were understood, it was too late to procure new sensors. It was therefore decided to fly the flight sensor and use cruise phase health check measurements to calibrate the temperature dependence of offset.

As sensor gain calibration was not possible during the mission, it was assumed the gain had not changed. Limited preflight measurements and more extensive calibration of the flight spare sensor suggested that the effects of gain changes on pressure measurements at 7 mbar were 6–8 times smaller than those of offset changes.

During the nominal landed mission, the ASI/MET pressure sensor experienced diurnal temperature variations of 265–300 K. These introduced large spurious components to the diurnal pressure cycle due to the temperature variation of sensor offset, which had to be removed using calibration data. In cruise, it was only possible to calibrate flight sensor pressure offset in the 270–280 K temperature range. These data indicated a temperature dependence of −0.019 mbar/K. This was the temperature dependence assumed by *Schofield et al.* [1997].

However, after the mission, the offset calibration was revisited. It was found that the cruise offset measurements were influenced by long-term changes (over 6 months) as well as temperature dependent changes. Offset measurements over the 270–280 K range made during the 90 min before entry eliminated the long-term drift and indicated a temperature dependence of −0.0135 mbar/K, a smaller dependence than the cruise offset measurements.

Late in the landed mission, when the spacecraft was off overnight and took data only during the day, the sensor temperature and measured pressure cycles were observed to be very similar from day-to-day (with the exception of the slow seasonal increase in pressure). However, during the four 24 hour, 4 s sampling sequences (sols 32, 38, 55, and 68), pressure sensor temperatures often differed by 15 K for the same time of day. This is because at the beginning of the sequence, the spacecraft has been off all night, while at the end of the sequence, it has been on all night. The −0.019 mbar/K temperature coefficient did not produce repeatable pressure cycles under these conditions, but the −0.0135 mbar/K coefficient did, providing additional support for the preentry result. The pressure cycle data also suggested that this offset coefficient was valid over the 260–310 K temperature range.

The revision of the pressure offset coefficient from −0.019 mbar/K used by *Schofield et al.* [1997] to −0.0135 mbar/K used in this work has changed the amplitude and phase of the diurnal tide reported by Schofield et al. (see text for details). However, the semidiurnal amplitude and phase have changed very little because the sensor temperature variation contains only a small semidiurnal component.

Acknowledgments. We are grateful to the Pathfinder flight team for their efforts on behalf of the ASI/MET experiment. We would also like to acknowledge Todd Clancy for providing our team access to some of his unpublished observations. Finally, the manuscript benefited greatly from comments by Francois Forget and an anonymous reviewer.

References

Arya, S. P., *Introduction to Micrometeorology*, Academic, San Diego, Calif., 1988.

Bougher, S. W., E. G. Fesen, E. C. Ridley, and R. W. Zurek, Mars mesosphere and thermosphere coupling: Semidiurnal tides, *J. Geophys. Res.*, *98*, 3281–3296, 1993.

Bridger, A. F. C., and J. R. Murphy, Mars' surface pressure tides and their behavior during global dust storms, *J. Geophys. Res.*, *103*, 8587–8601, 1998.

Christensen, P. R., et al., Results from the Mars Global Surveyor Thermal Emission Spectrometer, *Science*, *279*, 1692–1697, 1998.

Clancy, R. T., A. W. Grossman, M. J. Wolff, P. B. James, D. J. Rudy, Y. N. Billawala, B. J. Sandor, S. W. Lee, and D. O. Muhleman, Water vapor saturation at low altitudes around Mars aphelion: A key to Mars climate?, *Icarus*, *122*, 36–62, 1996.

Colaprete, A., O. B. Toon, and J. Magalhaes, Cloud formation under Mars Pathfinder conditions. *J. Geophys. Res.*, this issue.

Colburn, D. S., J. B. Pollack, and R. M. Haberle, Diurnal variations in optical depth at Mars, *Icarus*, *79*, 159–189, 1989.

Conrath, B. J., Thermal structure of the Martian atmosphere during the dissipation of the dust storms of 1971, *Icarus*, *24*, 36–46, 1975.

Edgett, K. S., and P. R. Christensen, Rocks and aeolian features in the Mars Pathfinder landing site region: Viking infrared thermal mapper observations, *J. Geophys. Res.*, *102*, 4107–4116, 1997.

Flaser, F. M., and R. M. Goody, Diurnal behavior of water on Mars, *Planet. Space. Sci.*, *24*, 161–181, 1976.

Forget, F., and J. B. Pollack, Thermal infrared observations of the condensing Martian polar caps: CO_2 ice temperatures and radiative budget, *J. Geophys. Res.*, *101*, 16,865–16,879, 1996.

Gierasch, P., and R. Goody, A study of the thermal and dynamical structure of the Martian lower atmosphere, *Planet. Space Sci.*, *16*, 615–646, 1968.

Golombek, M. P., et al., Overview of the Mars Pathfinder mission: Launch through landing, surface operations, data sets, and science results, *J. Geophys. Res.*, this issue.

Greeley, R., and J. D. Iversen, *Wind as a Geological Process*, 333 pp., Cambridge Univ. Press, New York, 1985.

Haberle, R. M., and B. M. Jakosky, Atmospheric effects on the remote determination of thermal inertia of Mars, *Icarus*, *90*, 187–204, 1991.

Haberle, R. M., H. C. Houben, R. Hertenstein, and T. Herdtle, A boundary layer for Mars: Comparison with Viking lander and entry data, *J. Atmos. Sci.*, *50*, 1544–1559, 1993.

Haberle, R. M., J. R. Barnes, J. R. Murphy, M. M. Joshi, and J. Schaeffer, Meteorological predictions for the Mars Pathfinder lander, *J. Geophys. Res.*, *102*, 13,301–13,311, 1997.

Hamilton, K. P., The effect of solar tides on the general circulation of the Martian atmosphere, *J. Atmos. Sci.*, *39*, 481–485, 1982.

Hayashi, J. N., B. M. Jakosky, and R. M. Haberle, Atmospheric effects on the mapping of Martian thermal inertia and thermally derived albedo, *J. Geophys. Res.*, *100*, 5277–5284, 1995.

Hourdin, F., F. Forget, and O. Talagrand, The sensitivity of the Martian surface pressure and atmospheric mass budget to various parameters: A comparison between numerical simulations and Viking observations, *J. Geophys. Res.*, *100*, 5501–5524, 1995.

Lewis, S. R., Validation of a Mars general circulation model against

recent observations from Mars Pathfinder and Mars Global Surveyor, *Ann. Geophys.*, *16*, C1000, 1998.

López-Valverde, M. A., D. P. Edwards, M. López-Puertas, and C. Roldán, Non–local thermodynamic equilibrium in general circulation models of the Martian atmosphere, 1, Effects of the local thermal equilibrium approximation on thermal cooling and solar heating, *J. Geophys. Res.*, *103*, 16,759–16,870, 1998.

Magalhaes, J. A., J. T. Schofield, and A. Seiff, Results of the Mars Pathfinder atmospheric structure investigation, *J. Geophys. Res.*, this issue.

Martin, T. Z., Thermal infrared opacity of the Martian atmosphere, *Icarus*, *66*, 2–21, 1986.

Mellor, G. L., and T. Yamada, Development of a turbulence closure model for geophysical fluid problems, *Rev. Geophys.*, *20*, 851–875, 1982.

Murphy, J. R., C. B. Leovy, and J. E. Tillman, Observations of Martian surface winds at the Viking Lander 1 site, *J. Geophys. Res.*, *95*, 14,555–14,576, 1990.

Pollack, J. B., C. B. Leovy, P. W. Greiman, and Y. Mintz, A Martian general circulation experiment with large topography, *J. Atmos., Sci.*, *38*, 3–29, 1981.

Pollack, J. B., R. M. Haberle, J. Schaeffer, and H. Lee, Simulations of the general circulation of the Martian atmosphere, 1, Polar processes, *J. Geophys. Res.*, *95*, 1447–1474, 1990.

Ryan, J. A., and R. D. Lucich, Possible dust devils: Vortices on Mars, *J. Geophys. Res.*, *88*, 11,005–11,011, 1983.

Savijarvi, H., Mars boundary layer modeling: Diurnal moisture cycle and soil properties at the Viking Lander 1 site, *Icarus*, *117*, 120–127, 1995.

Schofield, J. T., J. R. Barnes, D. Crisp, R. M. Haberle, J. A. Magalhaes, J. R. Murphy, A. Seiff, S. Larsen, and G. Wilson, The Mars Pathfinder atmospheric structure investigation/meteorology (ASI/MET) experiment, *Science*, *278*, 1752–1757, 1997.

Seiff, A., et al., The atmosphere structure and meteorology instrument on the Mars Pathfinder lander, *J. Geophys. Res.*, *102*, 4045–4056, 1997.

Smith, D. E., and M. T. Zuber, The shape of Mars and the topographic signature of the hemispheric dichotomy, *Science*, *271*, 184–188, 1996.

Smith, P. H., et al., Results from the Mars Pathfinder camera, *Science*, *278*, 1758–1764, 1997.

Sutton, J. L., C. B. Leovy, and J. E. Tillman, Diurnal variation of the Martian surface layer meteorological parameters during the first 45 sols at two Viking lander sites, *J. Atmos. Sci.*, *35*, 2346–2355, 1978.

Tillman, J., Mars global atmospheric oscillations: Annually synchronized, transient normal-mode oscillations and the triggering of global dust storms, *J. Geophys. Res.*, *93*, 9433–9451, 1988.

Toon, O. B., C. Sagan, and J. B. Pollack, Physical properties of the particles composing the Martian dust storm of 1971–1972, *Icarus*, *30*, 663–696, 1977.

Wilson, R. J., A general circulation model simulation of the Martian polar warming, *Geophys. Res. Lett.*, *24*, 123–126, 1997.

Wilson, R. J., and K. Hamilton, Comprehensive model simulation of thermal tides in the Martian atmosphere, *J. Atmos. Sci.*, *53*, 1290–1326, 1996.

Zurek, R. W., Atmospheric tidal forcing of the zonal-mean circulation: The Martian dusty atmosphere, *J. Atmos. Sci.*, *43*, 652–670, 1986.

Zurek, R. W., and R. M. Haberle, Zonally symmetric response to atmospheric tidal forcing in the dusty Martian atmosphere, *J. Atmos. Sci.*, *45*, 2469–2485, 1988.

J. R. Barnes, College of Oceanic and Atmospheric Sciences, Oregon State University, Corvallis, OR 97331.

A. F. C. Bridger, Department Meteorology, San Jose State University, San Jose, CA 95192.

R. M. Haberle and M. M. Joshi, Space Science Division, MS 245-3, NASA Ames Research Center, Moffett Field, CA 94035-1000. (bhaberle@mail.arc.nasa.gov)

J. L. Hollingsworth, San Jose State University Foundation, San Jose, CA 95192.

M. Lopez-Valverde, Instituto de Astrofisica de Andalucia, Apdo 3004, 18080 Granada, Spain.

J. R. Murphy, Department of Astronomy, New Mexido State University, Las Cruces, NM 87106.

J. Schaeffer, Raytheon Corp., Moffett Field, CA 94035-1000.

J. T. Schofield and G. Wilson, Jet Propulsion Laboratory, 4800 Oak Grove Drive, Pasadena, CA 91109.

(Received March 23, 1998; revised November 22, 1998; accepted November 25, 1998.)